Hypermetabolism, Hyperphagia, and Reduced Adiposity in Tankyrase-Deficient Mice

Tsung-Yin J. Yeh,[1] Kristina K. Beiswenger,[1] Pingping Li,[1] Krista E. Bolin,[2] Ray M. Lee,[3] Tsu-Shuen Tsao,[2] Anne N. Murphy,[4] Andrea L. Hevener,[5] and Nai-Wen Chi[1]

OBJECTIVE—Tankyrase (TNKS) is a Golgi-associated poly-ADP-ribose polymerase that is implicated in the regulation of GLUT4 trafficking in 3T3-L1 adipocytes. Its chromosomal locus 8p23.1 is linked to monogenic forms of diabetes in certain kindred. We hypothesize that TNKS is involved in energy homeostasis in mammals.

RESEARCH DESIGN AND METHODS—Gene-trap techniques were used to ablate TNKS expression in mice. Homozygous and wild-type littermates maintained on standard chow were compared.

RESULTS—Wild-type mice express the TNKS protein abundantly in adipose tissue, the brain, and the endocrine pancreas but scarcely in the exocrine pancreas and skeletal muscle. TNKS-deficient mice consume increased amounts of food (by 34%) but have decreased plasma leptin levels and a >50% reduction in epididymal and perirenal fat pad size. Their energy expenditure is increased as assessed by metabolic cage studies and core body temperatures. These changes are not attributable to an increase in physical activity or uncoupled respiration (based on oxygraph analyses of mitochondria isolated from brown fat and skeletal muscle). The heightened thermogenesis of TNKS-deficient mice is apparently fueled by increases in both fatty acid oxidation (based on muscle and liver gene expression analyses and plasma ketone levels) and insulin-stimulated glucose utilization (determined by hyperinsulinemic-euglycemic clamps). Although TNKS deficiency does not compromise insulin-stimulated GLUT4 translocation in primary adipocytes, it leads to the post-transcriptional upregulation of GLUT4 and adiponectin in adipocytes and increases plasma adiponectin levels.

CONCLUSIONS—TNKS-deficient mice exhibit increases in energy expenditure, fatty acid oxidation, and insulin-stimulated glucose utilization. Despite excessive food intake, their adiposity is substantially decreased. ***Diabetes*** **58:2476–2485, 2009**

Tankyrase (TNKS) is a modular protein with two distinct biochemical activities (1). The 20 copies of ankyrin repeats near the NH_2-terminus provide a pentavalent scaffold for diverse partners, most of which use the sequence motif RxxPDG to bind TNKS (2). The poly-ADP-ribose polymerase (PARP) domain at the COOH-terminus can modify TNKS and many of its partners through PARsylation. In this NAD-consuming reaction, acceptor proteins are covalently modified with polymers of ADP-ribose (PAR). The PARP activity of TNKS is constitutive and further enhanced by extracellular signal–related kinase (ERK)-mediated phosphorylation in cells stimulated with growth factors, supporting the notion that TNKS transduces phosphorylation cascades into PARsylation of effector proteins (3).

TNKS is implicated in diverse processes in cultured cells based partly on its subcellular localizations. In cycling cells, TNKS regulates telomere homeostasis and mitotic chromosomal segregation, consistent with its localization to the telomeres and spindle poles (1). In interphase, TNKS resides predominantly in the cytosol, often at sites of vesicular protein sorting (4). In 3T3-L1 adipocytes, for instance, TNKS concentrates at the Golgi area, where it colocalizes with GSVs (GLUT4 storage vesicles) (3). This colocalization suggests a potential role of TNKS in GLUT4 trafficking because GSVs are sorted at or near the Golgi into specialized compartments capable of insulin-stimulated exocytosis (5). Indeed, TNKS binds to the cytosolic tail of a GSV resident protein called IRAP (insulin-responsive aminopeptidase) (3). Moreover, in adipocytes treated with TNKS-specific siRNAs or a PARP inhibitor, insulin-stimulated GSV exocytosis and glucose uptake are both blunted (6). This effect is associated with impaired GSV targeting to exocytosis-competent compartments as assessed by membrane fractionation (6). Therefore, we speculated that TNKS-mediated PARsylation serves to generate a sorting tag on GSVs that guides the movement of these vesicles toward exocytosis-competent compartments (6). Interestingly, TNKS has been speculated as a candidate diabetes gene in humans (7) based on the linkage of its chromosomal locus, 8p23.1, to a subset of monogenic forms of type 2 diabetes (8,9). To directly implicate TNKS in energy homeostasis, we used a gene-trapping strategy to ablate TNKS expression in mice.

RESEARCH DESIGN AND METHODS

Trapping the TNKS gene. E14Tg2a.4, an embryonic stem cell line derived from 129/Ola mice, was electroporated with the GeneTrap Vector pGT1lxf and selected for G418 resistance at BayGenomics (http://baygenomics.ucsf.edu). The randomly trapped gene was identified by sequencing the resulting hybrid mRNA. Three embryonic stem clones (RRC239, RRA038, and XH267) containing a trapped TNKS allele were individually injected into C57BL/6 blastocysts. Female chimeric progenies were mated with wild-type C57BL/6 males. One chimera (RRC239) produced heterozygous offspring (50% 129, 50% C57BL/6). Pair mating between these heterozygotes and between their heterozygous progeny produced all the TNKS−/− mice and wild-type littermates used in this study.

Mouse care and handling. All procedures were approved by the Institutional Animal Care and Use Committee at the University of California, San Diego and Los Angeles. Up to four mice per cage were maintained in a controlled environment (23 ± 1°C, lights on from 6:00 A.M. to 6:00 P.M.) with free access to water and standard chow (Diet 5001, LabDiet, 13.5% of calories from fat).

From the [1]Department of Medicine, Endocrine Division, University of California, San Diego, La Jolla, California; the [2]Department of Biochemistry and Molecular Biophysics, University of Arizona, Tucson, Arizona; [3]Lestoni, Inc., Richmond, Virginia; the [4]Department of Pharmacology, University of California, San Diego, La Jolla, California; and the [5]Department of Medicine, University of California, Los Angeles, Los Angeles, California.

Corresponding author: Nai-Wen Chi, nwchi@ucsd.edu.

Received 22 December 2008 and accepted 14 July 2009. Published ahead of print at http://diabetes.diabetesjournals.org on 3 August 2009. DOI: 10.2337/db08-1781.

For respiratory spirometry, mice were individually housed in an 8-chamber Lab Animal Monitoring System (Oxymax, Columbus Instruments; 2,500-ml chamber, air flow at 680 ml/min, light cycle from 6:00 A.M. to 6:00 P.M.). After an 8-h acclimatization (10 A.M. to 6:00 P.M.), locomotor activity was monitored for 60 h using infrared motion detectors. Movement events (ambulatory plus Z-axis) were summed in 30-min intervals. At the end of each interval, O_2 consumption and CO_2 production were measured for 1 min. O_2 consumption was normalized to body weight raised to the 0.75th power as previously described (10). Each mouse was studied twice; the run that was associated with less body weight change was used for data analysis.

Mitochondrial isolation. Interscapular brown adipose tissue (BAT) from overnight-fasted mice was processed essentially as previously described (11) to obtain the mitochondrial fraction (~700 μg protein from ~100 mg tissue). Muscle (quadriceps, soleus, and gastrocnemius) from one leg was dissected free of tendons and fat and homogenized using a hand-held Polytron (7-mm generator probe, 5,000 rpm, for 4 s.) followed by a 10-ml Potter-Elvehjem Teflon/glass grinder (Wheaton) in a buffer consisting of 100 mmol/l KCl, 1 mmol/l EGTA, 5 mmol/l $MgSO_4$, and 50 mmol/l MOPS pH 7.4. The homogenates were centrifuged at 300*g* for 5 min to remove the nuclei. The supernatant was supplemented with 1 mmol/l ATP and 2 mg/ml BSA (fatty acid free, MP Biomedicals) and centrifuged at 8,000*g* for 10 min to obtain the mitochondria. The pellet was resuspended by adding 25 μl of a buffer consisting of 250 mmol/l sucrose, 0.1 mmol/l EGTA, and 10 mmol/l HEPES, pH 7.4. Aliquots of the mitochondrial fraction were solubilized in 1M NaOH for protein quantification using a Bio-Rad D_C kit or in SDS sample buffer for immunoblotting (20 μg/lane) using an anti-AIF antibody (Sigma) and a total OxPhos antibody cocktail (MitoSciences).

Mitochondrial oxygen consumption. The mitochondrial fraction (100 μg protein) was suspended and stirred in a polarographic oxygen chamber (Strathkelvin model 782) at 37°C. The chamber (100 μl) contained ADP (100 μmol/l) and complex I substrates (5 mmol/l glutamate, 2.5 mmol/l malate, 5 mmol/l pyruvate) along with either 100 mmol/l KCl, 2 mmol/l KH_2PO_4, 50 mmol/l Tris, pH 7.4, 5 mmol/l $MgCl_2$, 0.02 mmol/l EDTA, and 2 mg/ml BSA (for BAT mitochondria), or 250 mmol/l sucrose, 2 mmol/l KH_2PO_4, 10 mmol/l Tris, pH 7.4, 5 mmol/l $MgCl_2$, and 0.02 mmol/l EGTA (for muscle mitochondria). After oxygen consumption reached a steady rate (state 3), oligomycin (10 μg/ml, Sigma), and FCCP (carbonylcyanide-4-trifluoromethoxyphenyl-hydrazone, 300 nmol/l, Sigma) were added sequentially to measure state 4 and maximal (state 3u) respiration.

GLUT4 translocation and glucose uptake assays. After an overnight fast that began at 6:00 P.M., epididymal fat pads were harvested at 9:00 A.M. For glucose uptake assays, minced fat pads were digested with type 1 collagenase (120 unit/ml, Worthington Biochemical) essentially as previously described (12). After washing off the collagenase and removing undigested tissue using a 400-μm nylon mesh, adipocyte suspensions were stimulated with insulin (17 nmol/l, Sigma) for 30 min when indicated. [^{3}H]-deoxy-D-glucose was then added (0.2 μCi/ml, MP Biomedicals) for 10 min. Tracer uptake was determined as previously described (12) and normalized to protein content, which was quantified by lysing adipocytes in 1M NaOH. For subcellular fractionation, tissue was extensively minced in a buffer consisting of 131 mmol/l NaCl, 5 mmol/l KCl, 1 mmol/l $MgCl_2$, 2 mmol/l $CaCl_2$, 10 mmol/l HEPES, pH 7.4, 2.5 mmol/l NaH_2PO_4, 1% BSA (Sigma), and 1 mg/ml glucose. Insulin (17 nmol/l) was added when indicated, and samples were incubated at 37°C with constant rocking for 30 min. After being rinsed in ice-cold HES buffer (6), samples were homogenized in the same buffer using a 7-ml Dounce homogenizer (Wheaton). An aliquot was removed for immunoblotting, and the rest was subjected to differential centrifugation to purify the plasma membrane fraction as previously described (6).

Adiponectin oligomer analysis. Plasma (1 μl) was diluted in Tris-glycine native sample buffer (Invitrogen) and resolved in 7% Tris-acetate gels (Invitrogen) in a native running buffer (25 mmol/l Tris, 192 mmol/l glycine, pH 8.3). Samples were transferred onto nitrocellulose filters in the native running buffer supplemented with 20% methanol. The filters were blotted with rabbit antiserum (1:3,000) raised against the globular domain of mouse adiponectin and developed with a goat anti-rabbit antibody (1:5,000, LI-COR Biosciences) conjugated with an infrared fluorescence dye. Images were acquired using Odyssey Infrared System (LI-COR). The gel mobility of each adiponectin species was defined by comparison to purified bovine adiponectin whose oligomerization states were previously determined by mass spectrometry, equilibrium sedimentation, and gel-filtration chromatography (data not shown).

Adipose explant studies. Approximately 300 mg of epididymal fat tissue isolated from 12-month-old mice after an overnight fast (11:00 P.M. to 9:00 A.M.) was minced with scissors into ~40 pieces and rinsed in a strainer (100-μm pores, BD Falcon) with serum-free, low-glucose Dulbecco's modified Eagle's media containing 0.1% BSA. Tissue pieces were resuspended in 10 ml of the same medium in a polypropylene tube and gently rocked at 37°C in the presence of 5% CO_2. After 30 min of equilibration, fresh media was added (200 μl/100 mg tissue), and conditioned media was collected 2 h later for immunoblotting.

Immunoblotting. Frozen tissues were thawed in buffer A (3), homogenized using a Duall 20 glass grinder (Kontes), and clarified at 16,400 rpm for 10 min at 4°C. Supernatants were assayed in quadruplicate for protein content using a Bio-Rad D_C kit. For immunoblotting, the primary antibodies were against TNKS (H-350, 1 μg/ml, Santa Cruz), uncoupling protein (UCP)-1 (M17, 1:200, Santa Cruz), AMP-activated protein kinase α (total and p-Thr^{172} species, 1:1,000–2,000, Cell Signaling), RBP4 (1:2,000, Alpco Diagnostics), AdipoQ (1:750, Affinity Bioreagents), transthyretin (1:500, Abcam), ERp44 (1:500 [13]), and Ero1α (1:200; Santa Cruz). Antibodies against IRAP, sortilin, caveolin-1, and GLUT4 were previously described (6).

Islet morphometry. Images of pancreases sectioned at 50- to 100-μm intervals and stained with hematoxylin-eosin were analyzed using the Macnification software (Orbicule, Belgium). The cross-sectional areas of ~100 islets were averaged, and their proportion to the entire section was calculated.

RESULTS

Ablation of TNKS through gene trapping. The International Gene-Trap Consortium has generated a mouse embryonic stem cell library where each clone contains a random, intronic insertion of a vector that encodes a β-geo exon (conferring β-galactosidase activity) and a polyadenylation signal. Three clones from this library, each harboring the gene-trap vector in different TNKS introns, were expanded and injected into blastocysts. Germ-line transmission was achieved with one clone (RRC239), which expressed a hybrid mRNA where TNKS exon 1 was fused to the β-geo exon, indicative of gene trapping within intron 1. We localized the vector insertion site to nt. 891 of this intron (data not shown) and designed PCR primers to genotype chromosomal DNA (Fig. 1*A*).

When TNKS mRNA in the epididymal fat pads was quantified using real-time quantitative PCR (qPCR) that amplified the 3′ region, we found <5% of the wild-type level in mice homozygous for the trapped allele (data not shown). This allele is expected to express a severely truncated, nonfunctional TNKS protein fragment because exon 1 encodes only an incomplete copy of the ankyrin repeat (aa 192–217) preceded by a low-complexity region consisting primarily of His, Pro, and Ser residues (the HPS domain, aa 1–191). Therefore, we refer to the homozygotes as TNKS−/− mice or TNKS knockouts.

In wild-type mice, immunoblots revealed abundant TNKS expression in the pancreas, epididymal white adipose tissue (eWAT), periovarian fat (POF), interscapular brown fat (BAT), the lung, and the brain (Fig. 1*B*). The expression was modest in the liver and the heart but rather scarce in quadriceps muscle and the kidney. In TNKS−/− mice, the expression was ablated efficiently everywhere except in the brain. To localize TNKS expression within the pancreas, we applied X-gal histochemistry to TNKS−/− pancreases, taking advantage of the fact that the trapped allele allows the native TNKS promoter to express β-galactosidase as a fusion to TNKS exon 1. As a negative control, X-gal did not stain wild-type pancreases (Fig. 1*C*, *left panels*). In TNKS−/− pancreas, islets showed intense staining (Fig. 1*C*, *right upper panel*) whereas vascular walls showed modest staining (*right lower panel*). In contrast, no staining was discernable in exocrine acini, indicating that TNKS expression is largely confined to the endocrine pancreas. Within individual islets, the diffuse pattern of X-gal staining is characteristic of β-cells rather than α- or δ-cells, which typically reside in the islet periphery (14). The expression of TNKS in β-cells was confirmed by immunoblots of the insulinoma cell line INS-1 showing a higher TNKS abundance than in 3T3-L1

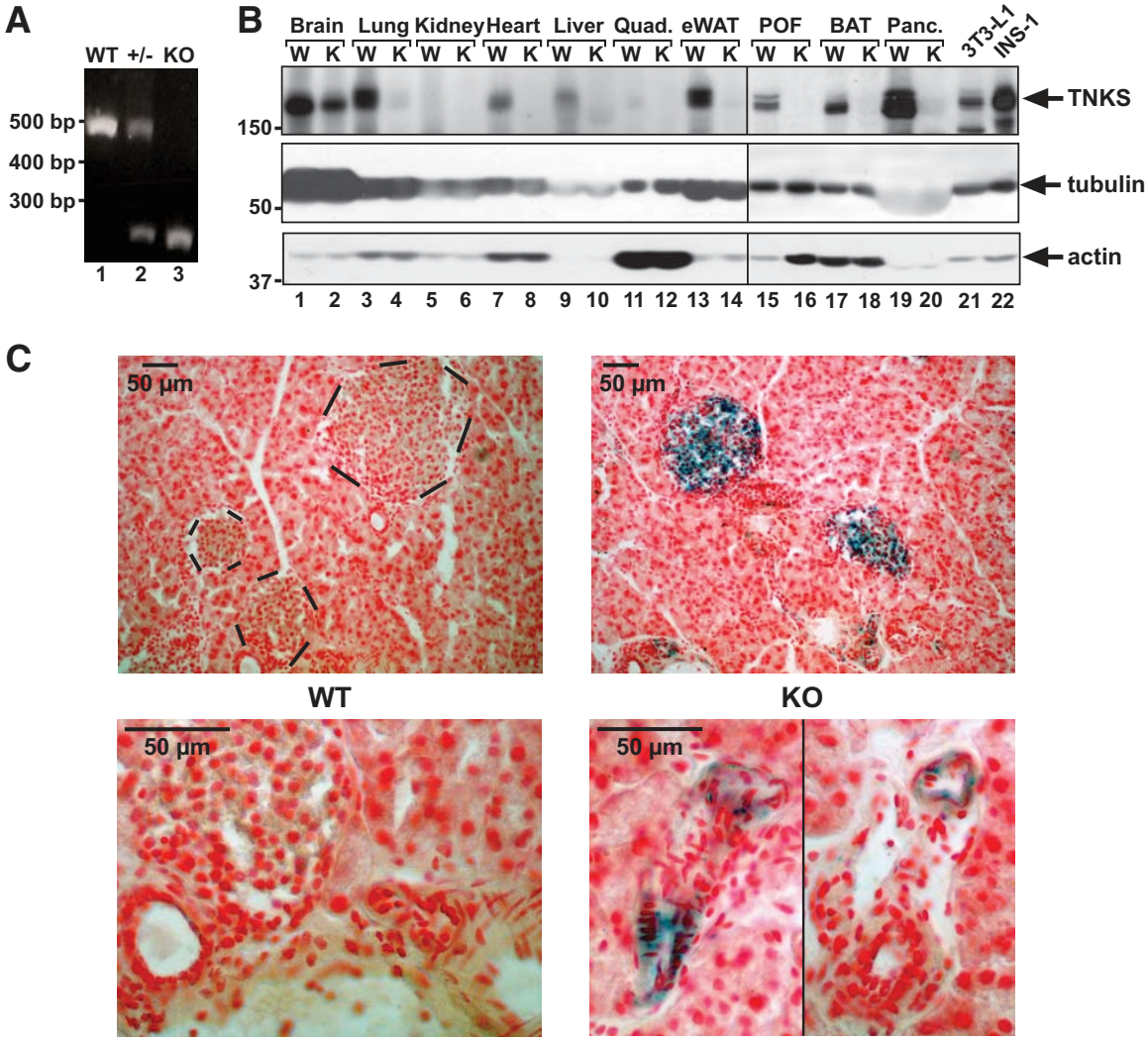

FIG. 1. TNKS expression and ablation. *A*: Mouse genotyping. DNA from the tails of wild-type mice and TNKS mutants (heterozygous +/−; homozygous −/−) was PCR amplified using the three primers as described in the supplementary Methods, available in the online appendix. The predicted product size is 470 bp for the wild type and 272 bp for the mutant allele. *B*: Protein extracts (40 μg/lane) of various organs from mice (1-month-old males in lanes 1–14; 2-month-old females in lanes 15–20) as well as cultured INS-1 cells and 3T3–L1 adipocytes (lanes 21–22) were immunoblotted for the indicated proteins. *C*: X-gal histochemistry. Cryosections (10-μm thick) of pancreas from 2-month-old wild-type (*left panels*) and TNKS−/− female mice (knockout, *right panels*) were fixed in 0.25% glutaraldehyde at room temperature for 15 min, stained at 37°C overnight with X-gal (which is hydrolyzed by β-galactosidase to a blue product), and counterstained with Nuclear Fast Red (Vector Labs) for 20 min. Digital images were acquired using a Nikon Eclipse 50*i* microscope. Broken lines delineate islets in the wild-type pancreas. *Lower panels* show high-power views of blood vessels (presumably arterioles) sectioned at various angles. The vertical line in the *right-lower panel* (and in subsequent figures) indicates regrouping of noncontiguous areas from the same exposure of a given slide (or a protein gel). K and KO, knockout; Panc., pancreas; Quad., quadriceps muscle; W and WT, wild type. (A high-quality color digital representation of this figure is available in the online issue.)

adipocytes (Fig. 1*B*, lane 22 vs. 21), heretofore considered the most TNKS-enriched cells (15).

TNKS−/− mice are hypermetabolic, hyperphagic, and lean. Among the 262 offspring produced by TNKS+/− parents, the genotype ratio (wild type: +/−: −/−) was 34:72:36 for males and 30:61:29 for females. Both were consistent with a Mendelian distribution ($P > 0.95$ by χ^2 test), indicating that genotype did not affect embryonic viability. In both sexes, TNKS−/− mice were overtly normal in appearance, fertility, and longevity. Unless otherwise specified, male TNKS knockouts and their wild-type littermates (age matched) were characterized in this study. All mice were derived from het-to-het crosses in a mixed genetic background (50% C57BL/6; 50% 129) and maintained on normal chow.

We found that adult TNKS−/− mice weighed 1.2 g less than wild type. The difference was not statistically significant (Fig. 2*A*), but the trend was discernable at as early as 10 weeks of age (supplementary Fig. S1, available in an online appendix at http://diabetes.diabetesjournals.org/cgi/content/full/db08-1781/DC1). The livers were smaller in TNKS knockouts, but the difference was not significant when normalized to body weight ($P > 0.15$). Heart sizes were comparable between genotypes. Notably, TNKS knockouts had a significant reduction in epididymal (eWAT) and perirenal fat pad (PRF) size (by 52 and 64%, respectively, Fig. 2*A*) as well as a 43% decrease in plasma leptin levels ($P = 0.014$, Fig. 2*B*), a marker of overall adiposity. The reduced adiposity was not associated with ectopic triglyceride accumulation in plasma, liver, or skeletal muscle (Fig. 2*C*). The leanness was clearly not because of inadequate food intake, as the knockouts actually consumed 34% more chow than the wild type ($P < 4 \times 10^{-6}$, Fig. 2*D*). Therefore, we

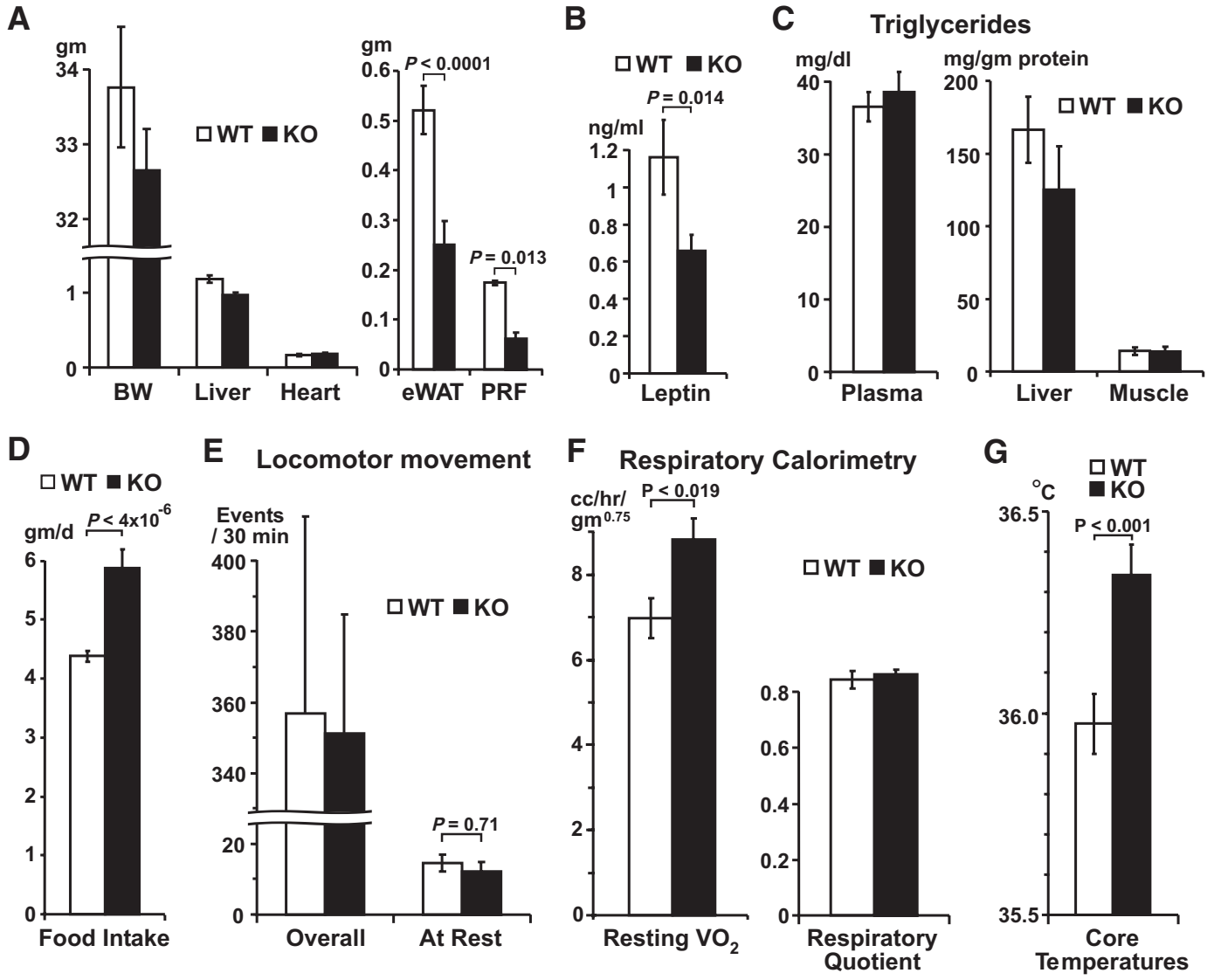

FIG. 2. TNKS−/− mice are lean, hyperphagic, and hypermetabolic. *A*: Body weight of male mice (aged 9–11 months; 25 wild type [WT], 23 knockout [KO]) and the mass of organs including eWAT and PRF of 12-month-old males (n = 14–15 per group, except n = 4–5 for PRF). In this and all other figures, error bars indicate ±SE. *B*: Fasting plasma leptin levels of male mice (aged 5–9 months; 18 wild type, 17 knockout). *C*: Triglyceride content of plasma (5-month-old males; 14 wild type, 11 knockout) and tissues (12-month-old males; 9 wild type, 7 knockout). *D*: Ad libitum food intake of individually housed male mice aged 9–11 months (23 wild type, 15 knockout) as determined by weighing the food pellets (twice a week) that remained above the grid. *E*: Movement events per 30-min interval. Male mice (11-month-old, 4 wild type, 8 knockout) were studied in metabolic cages. The overall frequency (on the left) represents the average between three dark cycles and two light cycles, totaling 120 intervals. The 10 intervals when individual mice showed the least movement were averaged to determine movement frequency at rest (on the right). *F*: Resting O_2 consumption (VO_2 normalized to [body weight]$^{0.75}$) and the respiratory quotient (VCO_2/VO_2) were determined during the same 10 intervals as in *E* when individual mice were least active physically. *G*: Rectal temperatures of 5–9 months old males (26 wild type, 21 knockout) were taken between 3 and 5:00 P.M. as previously described (36). Seven readings were taken for each mouse over a span of 5 weeks.

hypothesized that an increase in energy expenditure might explain why TNKS knockouts were lean despite hyperphagia.

To investigate energy expenditure, we used infrared beams in metabolic cages to quantify spontaneous movement in 30-min intervals for 2.5 days (120 intervals altogether). This revealed comparable overall locomotor activities between the two genotypes (Fig. 2*E*). Next, to specifically assess resting energy expenditure, we measured O_2 consumption during the 10 intervals (out of 120) when each mouse was least physically active. Interestingly, despite being equally inactive at rest (Fig. 2*E*), TNKS knockouts consumed 27% more O_2 than wild type ($P <$ 0.019, Fig. 2*F*), consistent with resting hypermetabolism. As an independent assessment of energy expenditure, we measured core body temperatures at 4:00 P.M., when mice were relatively inactive. We found significantly higher temperatures in TNKS knockouts (by 0.37°C, $P < 0.001$, Fig. 2*G*), again indicating resting hypermetabolism.

Mitochondrial respiration in TNKS−/− mice. Mouse models of increased energy expenditure often exhibit BAT expansion, UCP-1 overexpression in BAT, or uncoupled respiration in muscle (16–18). However, TNKS knockouts did not show any increases in BAT mass, UCP-1 protein content in BAT, or UCP-2 and -3 transcripts in BAT or muscle (Fig. 3*A–D*). To directly assess the coupling between substrate oxidation and ADP phosphorylation, we isolated mitochondria and measured O_2 consumption in the presence of ADP. Next, to measure respiration driven by proton leak alone, oligomycin was added to block oxidative phosphory-

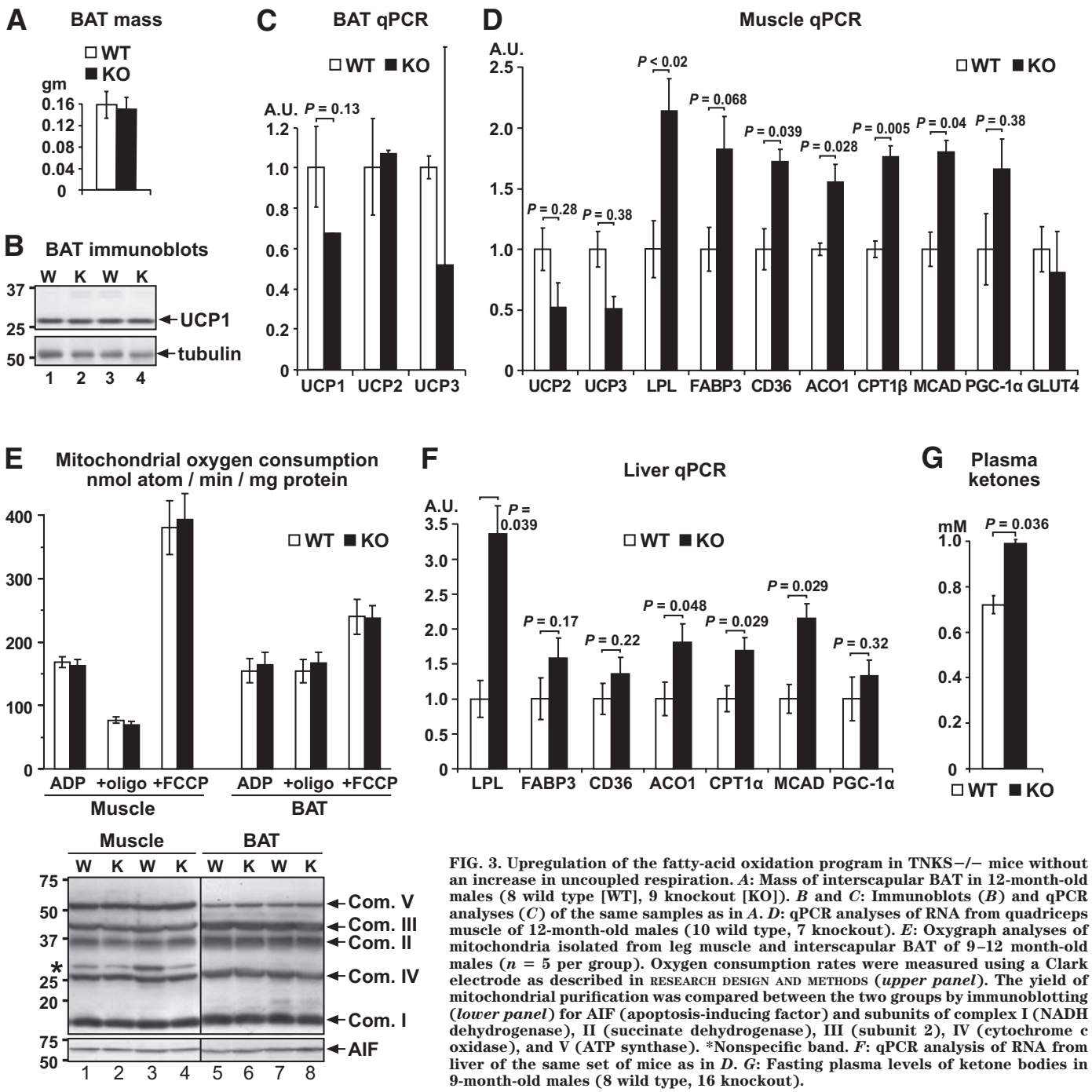

FIG. 3. Upregulation of the fatty-acid oxidation program in TNKS−/− mice without an increase in uncoupled respiration. *A*: Mass of interscapular BAT in 12-month-old males (8 wild type [WT], 9 knockout [KO]). *B* and *C*: Immunoblots (*B*) and qPCR analyses (*C*) of the same samples as in *A*. *D*: qPCR analyses of RNA from quadriceps muscle of 12-month-old males (10 wild type, 7 knockout). *E*: Oxygraph analyses of mitochondria isolated from leg muscle and interscapular BAT of 9–12 month-old males (n = 5 per group). Oxygen consumption rates were measured using a Clark electrode as described in RESEARCH DESIGN AND METHODS (*upper panel*). The yield of mitochondrial purification was compared between the two groups by immunoblotting (*lower panel*) for AIF (apoptosis-inducing factor) and subunits of complex I (NADH dehydrogenase), II (succinate dehydrogenase), III (subunit 2), IV (cytochrome c oxidase), and V (ATP synthase). *Nonspecific band. *F*: qPCR analysis of RNA from liver of the same set of mice as in *D*. *G*: Fasting plasma levels of ketone bodies in 9-month-old males (8 wild type, 16 knockout).

lation. Lastly, the uncoupling agent FCCP was added to assess maximal respiratory capacity. As anticipated, oligomycin inhibited respiration in muscle but not in BAT mitochondria (Fig. 3*E*), consistent with uncoupling proteins being maximally active in mitochondria isolated from BAT (19). Importantly, in both muscle and BAT mitochondria, TNKS knockout did not alter respiration rates under any condition (Fig. 3*E*). These data argue against mitochondrial uncoupling as the cause of increased energy expenditure in TNKS−/− mice.

Increased lipid utilization in TNKS−/− mice. To address which substrate(s) was used to fuel the heightened metabolism of TNKS−/− mice, we examined expression of the genes involved in lipid oxidation. In muscle, we observed significant overexpression of lipoprotein lipase (LPL), the gate keeper of tissue triglyceride utilization (20), as well as many genes involved in β-oxidation (21) including FAT/CD36 (for cellular fatty acid uptake), ACO1 (acyl-CoA oxidase, for peroxisomal β-oxidation), CPT-1 (for mitochondrial uptake of acyl CoA), and MCAD (medium-chain acyl-CoA dehydrogenase, for mitochondrial β-oxidation) (Fig. 3*D*). Many of these genes were also overexpressed in TNKS−/− liver (Fig. 3*F*), whereas those not directly involved in fatty acid oxidation (SREBP-1, HMG-CoA reductase, and the LDL receptor, data not shown) were not affected. Ketone bodies, the products of hepatic fatty acid oxidation, were also increased in TNKS−/− plasma (Fig. 3*G*). Collectively, these data suggest that increased fatty acid oxidation in muscle and liver contributes to the heightened metabolism of TNKS−/− mice.

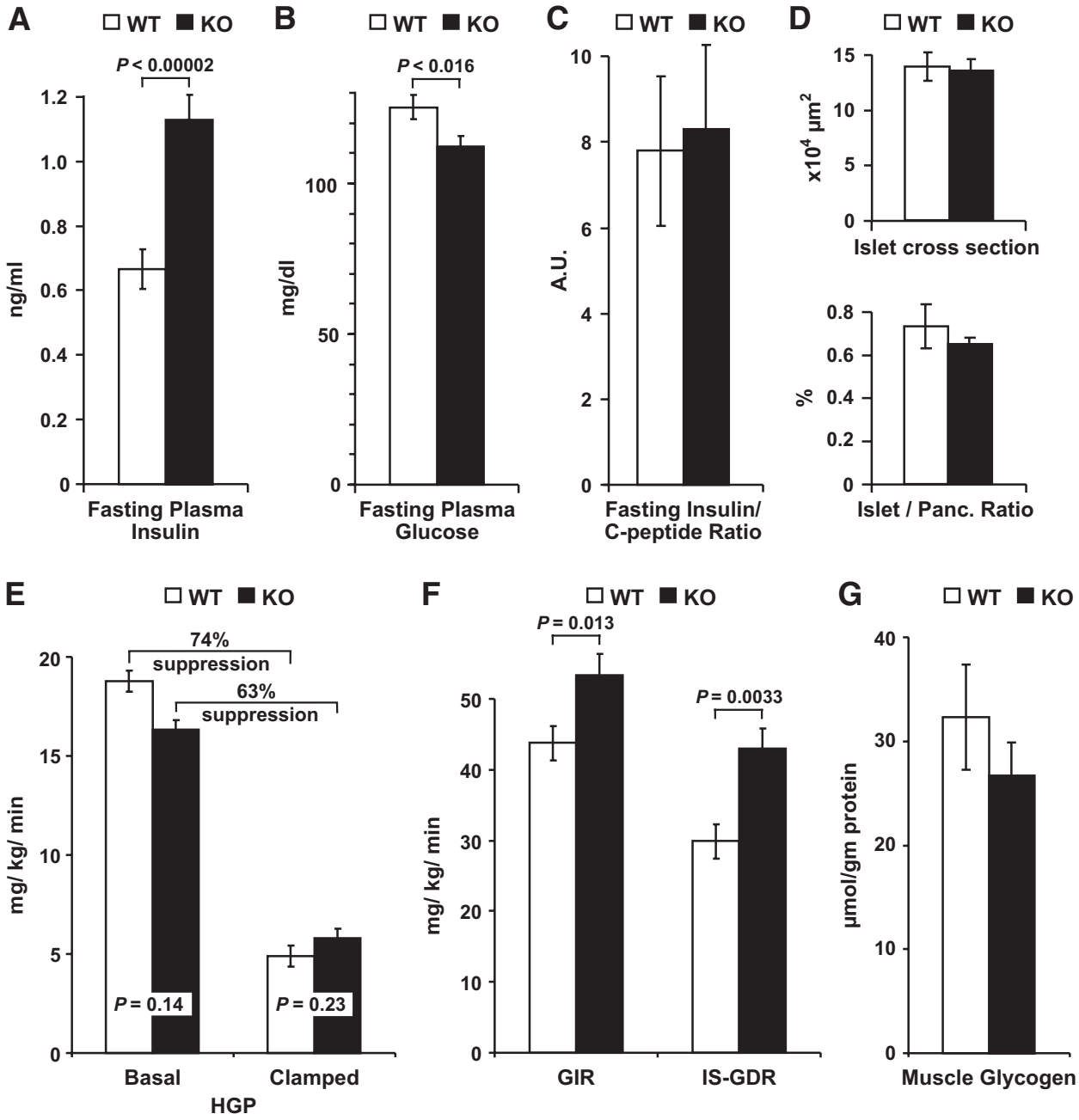

FIG. 4. TNKS−/− mice exhibit relative hypoglycemia and hyperinsulinemia in the fasting state and increased glucose disposal during hyperinsulinemic-euglycemic clamps. *A*: Fasting plasma insulin levels of 5-month-old males (23 wild type [WT], 26 knockout [KO]). *B*: Fasting plasma glucose levels of the same samples as in *A*. *C*: Insulin–to–C-peptide ratio in a subset of samples used in *A* is shown in arbitrary units (14 wild type, 15 knockout). *D*: Pancreases of 12-month-old males (5 wild type, 3 knockout) were analyzed for the cross-sectional area of individual islets (*upper panel*) and their areal proportion to the entire pancreas (*lower panel*). *E* and *F*: Hyperinsulinemic-euglycemic clamp studies were performed in 12-month-old male mice (9 wild type, 7 knockout) 3 days after the cannulation surgery. Mice were fasted for 6 h, placed in a restrainer to which they were acclimated, and studied in the conscious state essentially as described (37). Insulin was infused at 12 mU · kg^{-1} · min^{-1}, and whole-blood glucose was clamped around 100 mg/dl. HGP is shown in *E*. Glucose infusion rate (GIR) and IS-GDR are shown in *F*. *G*: Glycogen content (normalized to protein) of quadriceps muscle after hyperinsulinemic-euglycemic clamps (9 wild type, 7 knockout).

Fasting hyperinsulinemia and relative hypoglycemia in TNKS−/− mice. Increased fatty acid oxidation and ketogenesis could potentially result from insulin deficiency (22); however, this was not the case in TNKS−/− mice. Figure 4 shows that the fasting insulin levels of 5-month-old TNKS−/− mice were 70% higher than wild-type levels ($P < 0.00002$) whereas concomitant plasma glucose levels were 13 mg/dl lower ($P < 0.016$). These differences were also observed in 2-month-old males (supplemental Fig. S2), and the same trends were conserved in females (supplemental Fig. S3). The hyperinsulinemia was not associated with pancreatic islet expansion (Fig. 4*D*) and was not attributable to impaired insulin clearance given the normal ratio of this hormone to C-peptide (Fig. 4*C*). A likely explanation for the fasting hyperinsulinemia of TNKS−/− mice would be an exaggerated response of β-cells to ambient glucose, causing a decrease in the apparent homeostatic set-point for glucose. Similarly, in the fed state, the insulin levels of TNKS−/− mice were 30% higher than wild type while glucose levels were 8 mg/dl

lower (supplemental Fig. S4); however, neither difference reached statistical significance. These fed-state measurements were likely confounded by the hyperphagia of TNKS−/− mice.

Enhanced glucose disposal in TNKS−/− mice. To confirm that the hyperinsulinemia of TNKS−/− mice was not the result of insulin resistance, we measured glucose flux using hyperinsulinemic-euglycemic clamps. Figure 4*E* shows that TNKS−/− and wild-type mice had similar basal glucose turnover rates as determined by hepatic glucose production (HGP) (basal HGP, $P = 0.14$). During the clamp, the suppression of HGP was less complete in TNKS knockouts (63% vs. 74%, $P = 0.03$, Fig. 4*E*) but the difference was rather modest. More importantly, the glucose infusion rates (GIRs) required to maintain euglycemia during the clamps were 22% higher in TNKS−/− mice ($P = 0.013$), and their insulin-stimulated glucose disposal rates (IS-GDRs) were 44% higher than the wild type ($P = 0.003$, Fig. 4*F*). At the end of the clamps, the muscle glycogen content was comparable between the two genotypes (Fig. 4*G*), suggesting that the excess glucose uptake by TNKS−/− muscle (as inferred from IS-GDR) was committed to oxidation rather than stored as glycogen.

Hyperadiponectinemia in TNKS−/− mice. The role of adiponectin (adipoQ) in enhancing insulin sensitivity and fatty acid oxidation (23,24) prompted us to examine this adipokine in TNKS−/− mice. We found that TNKS−/− plasma has increased levels of both total adiponectin (Fig. 5*A*) and the high–molecular-weight species (Fig. 5*B*), the bioactive form (24). Consistent with increased adiponectin action, TNKS−/− muscle showed increased phosphorylation of AMPK (Fig. 5*C*), a mediator of adiponectin signaling (23). To explore the source of hyperadiponectinemia, we measured adipokine secretion from adipose explants ex vivo. Figure 5*D* shows increased adiponectin secretion from TNKS−/− explants compared to wild type, supporting a role of increased secretion in the hyperadiponectinemia of TNKS−/− mice. In contrast, another adipokine RBP4 (25) was secreted at a normal rate from TNKS−/− explants, suggesting that the decreased RBP4 levels in TNKS−/− plasma (Fig. 5*A*) were simply because of decreased adiposity. These changes in circulating adiponectin and RBP4 were detected at as early as 2 months of age (supplemental Fig. S2) and were apparently conserved in females (supplemental Fig. S3). The effect of TNKS knockout on adiponectin secretion was not attributable to changes in cellular levels of NAD (supplemental Fig. S5), a regulator of metabolism (26) whose concentration is modulated by TNKS overexpression in cultured cells (15).

Post-transcriptional adiponectin upregulation in TNKS−/− WAT. Adiponectin secretion is subject to a robust post-transcriptional regulation because of its efficient retention and degradation within the secretory pathway (13). Despite the hyperadiponectinemia of TNKS−/− mice, there was no increase in adiponectin mRNA levels (Fig. 6*A*). We also found no change in the expression of either ERp44 or Ero1-lα (Fig. 6*B*), chaperones that retain adiponectin in the endoplasmic reticulum (13,27,28). Interestingly, the adiponectin content of TNKS−/− fat pads, instead of being depleted by increased secretion, was actually higher than wild type (Fig. 6*B*, $P < 0.002$). In contrast to the post-transcriptional upregulation of adiponectin, the adipose content of other vesicular proteins (RBP4, IRAP, and sortilin) was not affected by TNKS knockout (Fig. 6*B*).

GLUT4 expression and translocation in TNKS−/− WAT. Unexpectedly, in tissues isolated at the end of the hyperinsulinemic-euglycemic clamps, we observed more GLUT4 protein in TNKS−/− WAT than in wild-type control (Fig. 6*B*) despite comparable mRNA levels (Fig. 6*A*). This was not associated with altered expression of Ubc9 (Fig. 6*A*), a protein implicated in GLUT4 stabilization (29), and was not observed in TNKS−/− muscle (Fig. 6*C*), a tissue with minimal TNKS expression (Fig. 1*B*). In the fasting state, we observed a smaller (24%, $P = 0.045$) increase in GLUT4 content in TNKS−/− WAT (Fig. 6*D*, lanes 1–2). Subcellular fractionation of WAT isolated from fasted mice showed more GLUT4 in the plasma membrane of TNKS−/− adipocytes compared to the wild type after insulin stimulation ex vivo (Fig. 6*D*, lane 4 vs. 6). However, the proportion of GLUT4 (relative to total GLUT4) that underwent insulin-stimulated translocation was not affected by TNKS knockout (Fig. 6*D*, bar graphs). Lastly, tracer glucose uptake assays showed that in insulin-stimulated TNKS−/− adipocytes, the anticipated increase in uptake compared to the wild type did not reach statistical significance (Fig. 6*E*). Nevertheless, the insulin-induced fold-change and increment in uptake were greater in TNKS−/− adipocytes than in the wild type ($P < 0.0005$ and $P = 0.12$, respectively, Fig. 6*E*). This difference is consistent with TNKS−/− adipocytes harboring an expanded pool of cellular GLUT4, the predominant mediator of insulin-induced glucose uptake.

DISCUSSION

TNKS deficiency impacts multiple aspects of energy metabolism in mice, leading to decreased adiposity despite increased food intake. This phenotype is attributable at least partly to heightened energy expenditure involving increased utilization of fatty acids and glucose. Our data do not support uncoupled mitochondrial respiration as the cause for decreased adiposity in TNKS−/− mice. Instead, a more plausible explanation is that a higher ATP demand drives increased combustion of fuel. This increased demand could potentially arise from various futile (ATP-dissipating) cycles such as calcium cycling across endoplasmic reticulum membranes and reversible protein modifications (16,30). Although it is possible that the decreased adiposity reflects an altered neural set-point for energy homeostasis, TNKS−/− mice differ from established models of CNS-mediated lean mice in that the latter often consume less food and are physically more active (31). Lastly, decreased adiposity could also result from an impairment in adipose storage function (31). However, other consequences of dysfunctional adipocytes such as hepatic steatosis, insulin resistance, and decreased plasma adiponectin (32) were not observed in TNKS−/− mice.

Because TNKS is expressed in multiple endocrine organs, tissue-selective knockouts would be required to specify the cell type in which TNKS plays a direct role in systemic energy homeostasis. In the current knockout model, the fasting hyperinsulinemia and relative hypoglycemia (Fig. 4) could indicate a β-cell–specific effect of TNKS ablation on insulin secretion, causing a shift in the homeostatic set-point for glucose. Alternatively, the impact on β-cell function could be secondary to systemic effects arising from TNKS ablation elsewhere. As for the hyperadiponectinemia of TNKS−/− mice (Fig. 5), we speculate that TNKS ablation exerts an adipocyte-specific effect at the post-transcriptional level. Whether this in-

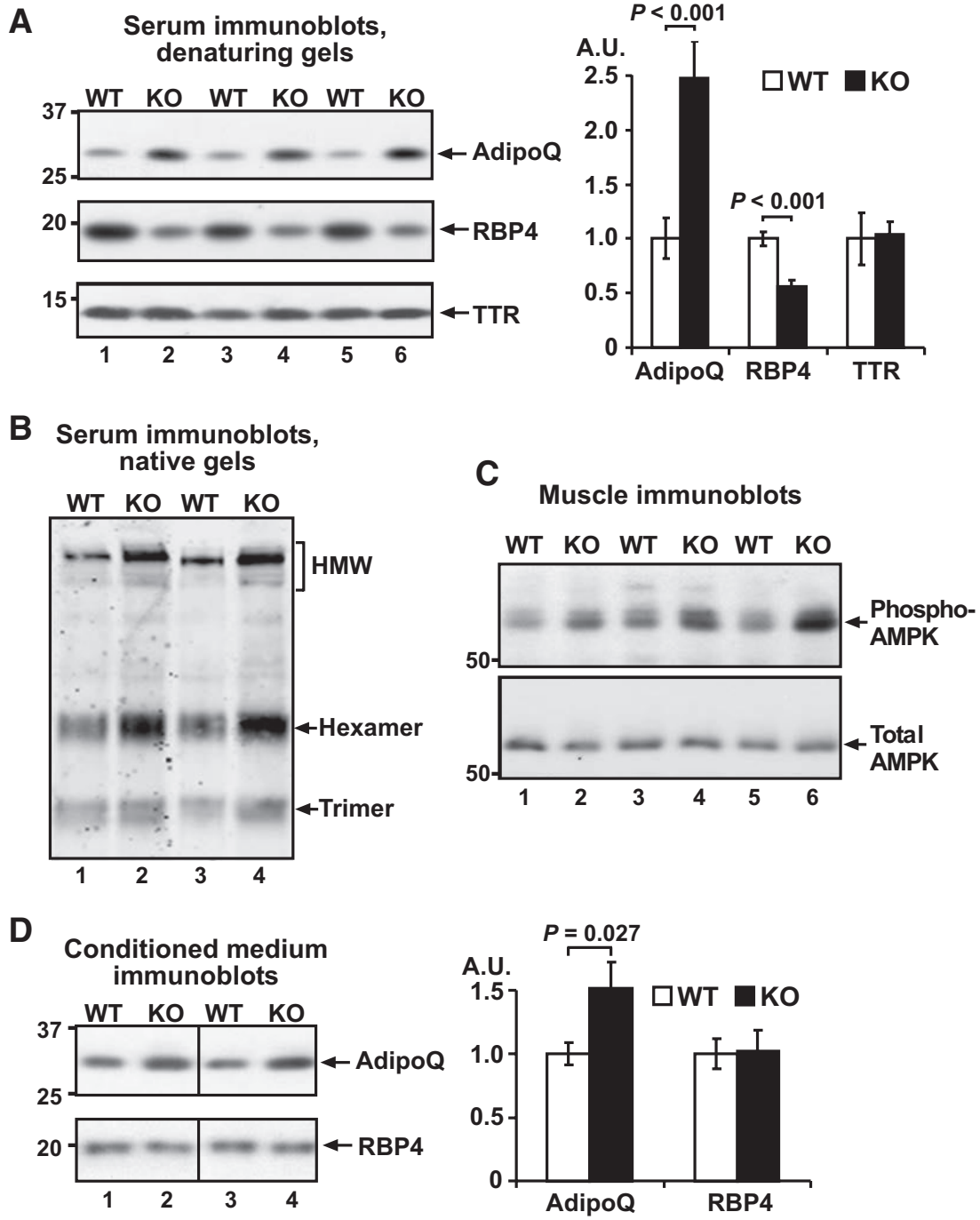

FIG. 5. Effects of TNKS knockout on adipokines in plasma and explant-conditioned media. *A*: Fasting plasma from 5-month-old males (17 wild type [WT], 20 knockout [KO]) was resolved by SDS-PAGE and immunoblotted for adiponectin (AdipoQ), RBP4, and transthyretin (TTR), a carrier protein that stabilizes RBP4 in circulation (25). Densitometry quantification and representative blots are shown. *B*: The same samples as in *A* were resolved in native (nonreducing, nondenaturing) gels as described in RESEARCH DESIGN AND METHODS and immunoblotted for various adiponectin complexes. *C*: Muscle samples from Fig. 4*G* were immunoblotted using antibodies against AMPK (*lower panel*) and phospho-Thr^{172} AMPK (*upper panel*). *D*: Media conditioned by epididymal fat pads freshly isolated from 12-month-old males (5 wild type, 4 knockout) as described in RESEARCH DESIGN AND METHODS were immunoblotted (30 μl/lane) for adiponectin and RBP4 and quantified as in *A*.

volves increased translation of adiponectin mRNA or stabilization of the adipokine in the secretory pathway remains to be investigated. Given the susceptibility of nascent adiponectin to degradation in the secretory pathway (13) and the localization of TNKS to the Golgi of adipocytes (3), it is plausible that TNKS ablation stabilizes intracellular adiponectin by redirecting the vesicular movement of the adipokine. Similar mechanisms could also account for the post-transcriptional upregulation of GLUT4 in TNKS−/− WAT (Fig. 6). Although the ensuing hyperadiponectinemia could secondarily impact skeletal muscle and other tissues, leading to the increases in fatty acid oxidation and insulin sensitivity as observed in TNKS−/− mice (Figs. 3 and 4), additional studies are required to directly implicate adiponectin in the phenotype of TNKS−/− mice.

Primary adipocytes isolated from our TNKS knockout model do not exhibit the impaired GLUT4 translocation

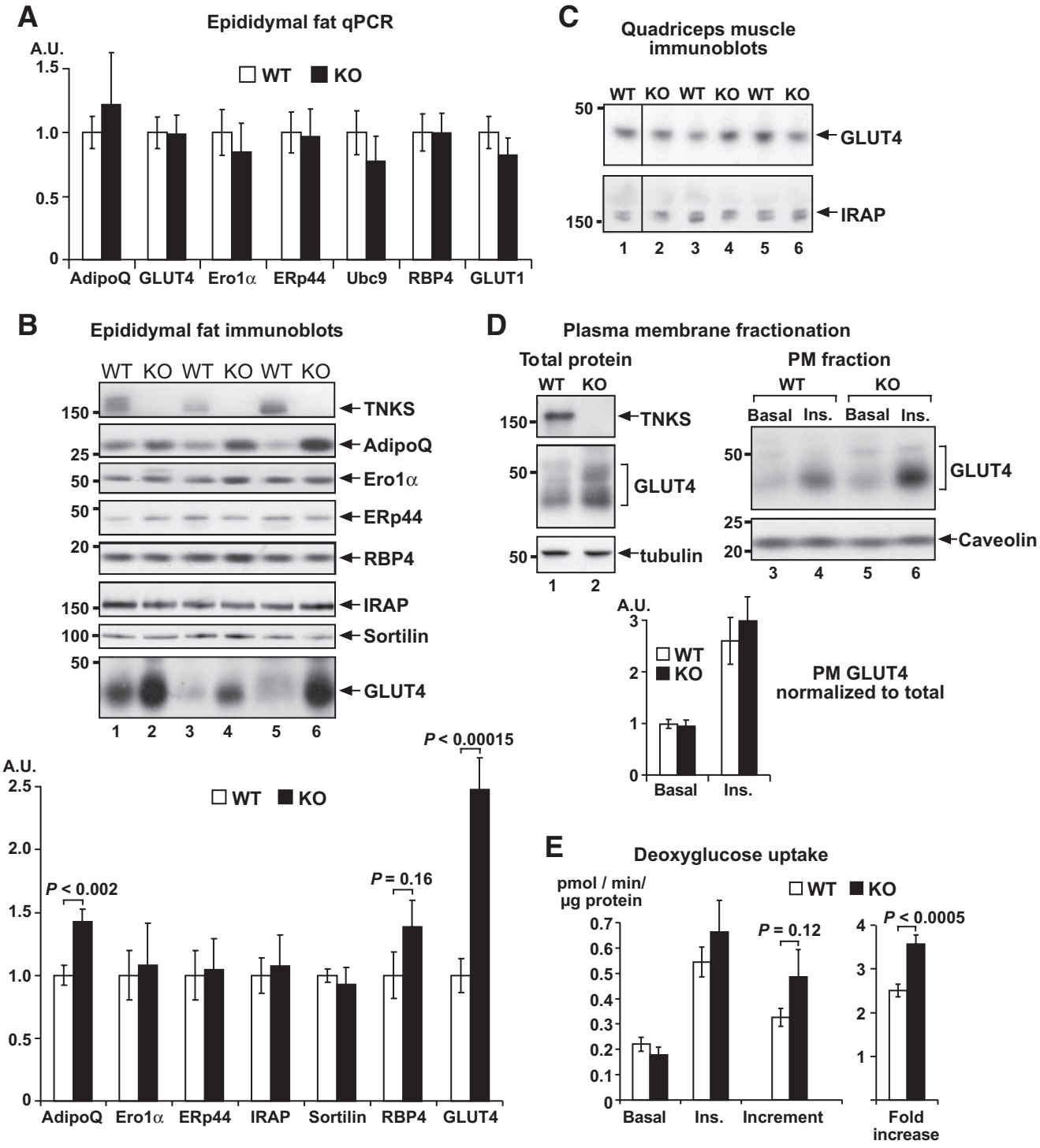

FIG. 6. Effects of TNKS knockout on gene expression and GLUT4 translocation in adipocytes. *A–C*: Epididymal fat pads and quadriceps muscle of 12-month-old mice (10 wild type [WT], 7 knockout [KO]) were harvested at the end of hyperinsulinemic-euglycemic clamps for qPCR analysis (*A*) and immunoblotting (*B* and *C*). Densitometry analysis and representative blots are shown. *D* and *E*: Adipocytes harvested from epididymal fat pads of 9- to 12-month-old male mice after an overnight fast were stimulated ex vivo with insulin (17 nmol/l, 30 min) and subjected to plasma-membrane fractionation (5 wild type, 5 knockout) or deoxyglucose uptake analyses (9 wild type, 7 knockout) as described in RESEARCH DESIGN AND METHODS. *D*: Representative immunoblots of total cellular proteins and the plasma membrane (PM) fraction. The bar graph shows average plasma membrane GLUT4 content normalized to total GLUT4 content. *E*: [^{3}H]-2-deoxy-D-glucose uptake rates were normalized to cellular protein content in basal and insulin-stimulated states. The difference and the ratio between these two values for each mouse are expressed as insulin-induced increment and fold-increase in glucose uptake, respectively.

that would be expected from the effects of TNKS siRNAs on 3T3-L1 adipocytes (6). In a separate TNKS knockout model (33), adipocytes also did not exhibit defects in glucose uptake, and lymphocytes did not display the changes in mitotic progression or telomere length that would be predicted from studies involving cultured cells (1). In both mouse models, the impact of TNKS deficiency on certain cellular processes was likely masked by compensatory mechanisms not available to cultured cells. Nevertheless, the robust changes in energy homeostasis in

TNKS−/− mice suggest the possibility that pharmacological inhibition of TNKS, particularly its PARP activity, could ameliorate obesity and improve insulin sensitivity.

ACKNOWLEDGMENTS

This work was supported in part by grants from the American Diabetes Association (7-05-CD-05 to N.-W.C.; 1-08-JF-54 to T.-S.T.) and the National Institutes of Health (T32 DK-007044 to T.-Y.J.Y.; DK-073227 and DK-060484 to A.L.H.).

No potential conflicts of interest relevant to this article were reported.

We thank Dr. Susanna R. Keller (University of Virginia) and Dr. Theodore P. Ciaraldi (University of California, San Diego [UCSD]) for enlightening discussions; Dr. Philipp Scherer (University of Texas) for advice and ERp44 antibody; Xin Yu (University of California, Davis) for generating TNKS+/− mice from embryonic stem cell clones; Laarni Gapuz (UCSD) for X-gal histochemistry; Margo Streets (UCSD) for metabolic cage studies; Dr. Young-Sun Hong (UCSD) and Susanna Petrosyan (UCSD) for technical advice.

REFERENCES

1. Hsiao SJ, Smith S. Tankyrase function at telomeres, spindle poles, and beyond. Biochimie 2008;90:83–92
2. Sbodio JI, Chi NW. Identification of a tankyrase-binding motif shared by IRAP, TAB182, and human TRF1 but not mouse TRF1. NuMA contains this RxxPDG motif and is a novel tankyrase partner. J Biol Chem 2002;277:31887–31892
3. Chi NW, Lodish HF. Tankyrase is a Golgi-associated mitogen-activated protein kinase substrate that interacts with IRAP in GLUT4 vesicles. J Biol Chem 2000;275:38437–38444
4. Yeh TY, Meyer TN, Schwesinger C, Tsun ZY, Lee RM, Chi NW. Tankyrase recruitment to the lateral membrane in polarized epithelial cells: regulation by cell-cell contact and protein poly(ADP-ribosyl)ation. Biochem J 2006;399:415–425
5. Bryant NJ, Govers R, James DE. Regulated transport of the glucose transporter GLUT4. Nat Rev Mol Cell Biol 2002;3:267–277
6. Yeh TY, Sbodio JI, Tsun ZY, Luo B, Chi NW. Insulin-stimulated exocytosis of GLUT4 is enhanced by IRAP and its partner tankyrase. Biochem J 2007;402:279–290
7. Dunn JS, Mlynarski WM, Pezzolesi MG, Borowiec M, Powers C, Krolewski AS, Doria A. Examination of PPP1R3B as a candidate gene for the type 2 diabetes and MODY loci on chromosome 8p23. Ann Intern Med 2006;70:587–593
8. Pezzolesi MG, Nam M, Nagase T, Klupa T, Dunn JS, Mlynarski WM, Rich SS, Warram JH, Krolewski AS. Examination of candidate chromosomal regions for type 2 diabetes reveals a susceptibility locus on human chromosome 8p23.1. Diabetes 2004;53:486–491
9. Kim SH, Ma X, Weremowicz S, Ercolino T, Powers C, Mlynarski W, Bashan KA, Warram JH, Mychaleckyj J, Rich SS, Krolewski AS, Doria A. Identification of a locus for maturity-onset diabetes of the young on chromosome 8p23. Diabetes 2004;53:1375–1384
10. Even PC, Mokhtarian A, Pele A. Practical aspects of indirect calorimetry in laboratory animals. Neurosci Biobehav Rev 1994;18:435–447
11. Cunningham SA, Wiesinger H, Nicholls DG. Quantification of fatty acid activation of the uncoupling protein in brown adipocytes and mitochondria from the guinea pig. Eur J Biochem 1986;157:415–420
12. Qi L, Saberi M, Zmuda E, Wang Y, Altarejos J, Zhang X, Dentin R, Hedrick S, Bandyopadhyay G, Hai T, Olefsky J, Montminy M. Adipocyte CREB promotes insulin resistance in obesity. Cell Metab 2009;9:277–286
13. Wang ZV, Schraw TD, Kim JY, Khan T, Rajala MW, Follenzi A, Scherer PE. Secretion of the adipocyte-specific secretory protein adiponectin critically depends on thiol-mediated protein retention. Mol Cell Biol 2007;27:3716–3731
14. Orci L, Unger RH. Functional subdivision of islets of Langerhans and possible role of D cells. Lancet 1975;2:1243–1244
15. Yeh TY, Sbodio JI, Nguyen MT, Meyer TN, Lee RM, Chi NW. Tankyrase-1 overexpression reduces genotoxin-induced cell death by inhibiting PARP1. Mol Cell Biochem 2005;276:183–192
16. Silva JE. Thermogenic mechanisms and their hormonal regulation. Physiol Rev 2006;86:435–464
17. Gesualdo L, Ranieri E, Monno R, Rossiello MR, Colucci M, Semeraro N, Grandaliano G, Schena FP, Ursi M, Cerullo G. Angiotensin IV stimulates plasminogen activator inhibitor-1 expression in proximal tubular epithelial cells. Kidney Int 1999;56:461–470
18. Bianco AC, Salvatore D, Gereben B, Berry MJ, Larsen PR. Biochemistry, cellular and molecular biology, and physiological roles of the iodothyronine selenodeiodinases. Endocr Rev 2002;23:38–89
19. Shabalina IG, Jacobsson A, Cannon B, Nedergaard J. Native UCP1 displays simple competitive kinetics between the regulators purine nucleotides and fatty acids. J Biol Chem 2004;279:38236–38248
20. Merkel M, Eckel RH, Goldberg IJ. Lipoprotein lipase: genetics, lipid uptake, and regulation. J Lipid Res 2002;43:1997–2006
21. Eaton S. Control of mitochondrial β-oxidation flux. Prog Lipid Res 2002;41:197–239
22. Sidossis LS, Stuart CA, Shulman GI, Lopaschuk GD, Wolfe RR. Glucose plus insulin regulate fat oxidation by controlling the rate of fatty acid entry into the mitochondria. J Clin Invest 1996;98:2244–2250
23. Yamauchi T, Kamon J, Minokoshi Y, Ito Y, Waki H, Uchida S, Yamashita S, Noda M, Kita S, Ueki K, Eto K, Akanuma Y, Froguel P, Foufelle F, Ferre P, Carling D, Kimura S, Nagai R, Kahn BB, Kadowaki T. Adiponectin stimulates glucose utilization and fatty-acid oxidation by activating AMP-activated protein kinase. Nat Med 2002;8:1288–1295
24. Kadowaki T, Yamauchi T, Kubota N, Hara K, Ueki K, Tobe K. Adiponectin and adiponectin receptors in insulin resistance, diabetes, and the metabolic syndrome. J Clin Invest 2006;116:1784–1792
25. Yang Q, Graham TE, Mody N, Preitner F, Peroni OD, Zabolotny JM, Kotani K, Quadro L, Kahn BB. Serum retinol binding protein 4 contributes to insulin resistance in obesity and type 2 diabetes. Nature 2005;436:356–362
26. Sauve AA. NAD+ and vitamin B3: from metabolism to therapies. J Pharmacol Exp Ther 2008;324:883–893
27. Wang Y, Lam KS, Yau MH, Xu A. Post-translational modifications of adiponectin: mechanisms and functional implications. Biochem J 2008;409:623–633
28. Qiang L, Wang H, Farmer SR. Adiponectin secretion is regulated by SIRT1 and the endoplasmic reticulum oxidoreductase Ero1-L-α. Mol Cell Biol 2007;27:4698–4707
29. Giorgino F, de Robertis O, Laviola L, Montrone C, Perrini S, McCowen KC, Smith RJ. The sentrin-conjugating enzyme mUbc9 interacts with GLUT4 and GLUT1 glucose transporters and regulates transporter levels in skeletal muscle cells. Proc Natl Acad Sci U S A 2000;97:1125–1130
30. She P, Reid TM, Bronson SK, Vary TC, Hajnal A, Lynch CJ, Hutson SM. Disruption of BCATm in mice leads to increased energy expenditure associated with the activation of a futile protein turnover cycle. Cell Metab 2007;6:181–194
31. Reitman ML. Metabolic lessons from genetically lean mice. Annu Rev Nutr 2002;22:459–482
32. Reue K, Phan J. Metabolic consequences of lipodystrophy in mouse models. Curr Opin Clin Nutr Metab Care 2006;9:436–441
33. Chiang YJ, Hsiao SJ, Yver D, Cushman SW, Tessarollo L, Smith S, Hodes RJ. Tankyrase 1 and tankyrase 2 are essential but redundant for mouse embryonic development. PLoS ONE 2008;3:e2639
34. Passonneau JV, Lauderdale VR. A comparison of three methods of glycogen measurement in tissues. Anal Biochem 1974;60:405–412
35. Pfaffl MW, Horgan GW, Dempfle L. Relative expression software tool (REST) for group-wise comparison and statistical analysis of relative expression results in real-time PCR. Nucleic Acid Res 2002;30:e36
36. Miller DB, O'Callaghan JP. Environment-, drug- and stress-induced alterations in body temperature affect the neurotoxicity of substituted amphetamines in the C57BL/6J mouse. J Pharmacol Exp Ther 1994;270:752–760
37. Lee CH, Olson P, Hevener A, Mehl I, Chong LW, Olefsky JM, Gonzalez FJ, Ham J, Kang H, Peters JM, Evans RM. PPAR-Δ regulates glucose metabolism and insulin sensitivity. Proc Natl Acad Sci U S A 2006;103:3444–3449